

Focus on the Essential: Extracting the Decisive Energy Barrier of a Complex Process

Simon Aeschlimann, Julia Neff, Ralf Bechstein, Chiara Paris, Andrea Floris, Lev Kantorovich, and Angelika Kühnle*

Molecular processes at surfaces can be composed of a rather complex sequence of steps. The kinetics of even seemingly simple steps are demonstrated to depend on a multitude of factors, which prohibits applying a simple Arrhenius law. This complexity can make it challenging to experimentally determine the kinetic parameters of a single step. However, a molecular-level understanding of molecular processes such as structural transitions requires elucidating the atomistic details of the individual steps. Here, a strategy is presented to extract the energy barrier of a decisive step in a very complex structural transition by systematically addressing all factors that impact the transition kinetics. Only by eliminating these factors in the measurement the experimental data will follow an Arrhenius law and the barrier can be extracted for the single step. Using the system of 2,5-dihydroxybenzoic acid on calcite (10.4) as an example, the energy barrier is determined for the attachment-assisted dissociation of molecular dimers in the structural transition from a striped to a dense molecular surface structure. This disentanglement approach is mandatory for a direct comparison with theoretical results and provides molecular-level insights into the transition mechanism.

The quantitative understanding of the kinetics of atomic and molecular processes at surfaces is pivotal to many fields, e.g., within epitaxy,^[1–3] catalysis,^[4–7] switches and sensor applications^[8–10] or smart materials.^[11]

Investigating the kinetics of molecular processes at surfaces allows determining the energy barriers of the steps involved.^[12,13] When the process of interest can be directly followed by an experimental technique, the kinetics of the process might be accessible. As an example, scanning tunneling microscopy (STM) provides the capability to determine the barrier of a very fundamental surface process, namely diffusion of atoms^[14,15] and molecules^[16,17] on metal surfaces.^[18] In many of these studies, the barrier of this single step can be deduced in an elegant and simple fashion from a direct measurement of the hopping events as a function of the temperature.

Microscopy techniques can also shed light on the kinetics in systems where the reaction is accompanied by a change in the relative surface coverage, e.g., for lipase enzymes that degrade surface-supported lipid bilayers,^[19,20] photoinduced switching^[21] or the growth of graphene flakes.^[22] Another example focusses on the chemical exchange reaction kinetics between two different epoxy networks that has been determined by recording the temperature-dependent interfacial broadening.^[23] Besides microscopy, other methods such as the quartz-crystal microbalance have been used to monitor the formation kinetics of lipid bilayers from vesicles bilayer^[24,25] and the change in mass has been measured to follow the growth of nanowires on a copper surface.^[26] These elegant examples do, however, require the process of interest to be directly reflected in a measurable quantity, e.g., the hopping frequency, the change of the surface coverage, or interfacial broadening, which allows applying a simple Arrhenius approach to determine the barrier. However, in many cases—as in the present work—the situation can be considerably more complex and the Arrhenius law fails to describe the kinetics of the complete process. Complex processes, in contrast to the simple examples presented above, depend on various factors.^[27,28] As an example, it is well known that even simple adsorbate diffusion usually depends on the coverage.^[14] Moreover, for many surface reactions complex pathways involving transition states have been revealed.^[29] In the latter case, recording an


S. Aeschlimann, Prof. J. Neff
Institute of Physical Chemistry
Johannes Gutenberg University Mainz
Duesbergweg 10-14, 55099 Mainz, Germany

S. Aeschlimann
Graduate School Materials Science in Mainz
Staudingerweg 9, 55128 Mainz, Germany

Dr. R. Bechstein, Prof. A. Kühnle
Physical Chemistry I
Department of Chemistry
Bielefeld University
Universitätsstraße 25, 33615 Bielefeld, Germany
E-mail: kuehnle@uni-bielefeld.de

Dr. C. Paris, Dr. A. Floris, Prof. L. Kantorovich
Department of Physics
King's College London
London WC2R 2LS, UK

Dr. A. Floris
School of Chemistry
University of Lincoln
Brayford Pool, Lincoln LN6 7TS, UK

 The ORCID identification number(s) for the author(s) of this article can be found under <https://doi.org/10.1002/admi.201900795>.

© 2019 The Authors. Published by WILEY-VCH Verlag GmbH & Co. KGaA, Weinheim. This is an open access article under the terms of the Creative Commons Attribution-NonCommercial License, which permits use, distribution and reproduction in any medium, provided the original work is properly cited and is not used for commercial purposes.

DOI: 10.1002/admi.201900795

averaged observable results in monitoring an effective reaction rate due to several involved steps. This can make it challenging to disentangle the kinetics of the involved steps and, thus, determine the corresponding individual energy barriers. Therefore, the barrier of a single step of interest might not be experimentally accessible in a straightforward manner. In turn, this makes it difficult or even impossible to compare experimentally determined energy barriers with theoretical simulations. A possible approach is to greatly simplify the system under investigation, e.g., when studying catalytic processes at surfaces, a reaction in the gas phase is investigated instead.^[5] However, this approach, as a matter of principle, cannot capture the mechanistic and kinetic details that govern the processes at the surface. In contrast, our disentanglement approach is to leave the system unchanged but design the experimental conditions in a way that information on individual steps can be disclosed.

In general, to determine the energy barrier of a process step, the temperature dependence of the respective rate constant has to be measured. Knowing the detailed process pathway, the experimental conditions can be adjusted to focus on the specific step of interest and to elucidate the molecular-scale mechanisms. A prime example to illustrate the complexity of structural transitions and corresponding rates is given by 2,5-dihydroxybenzoic acid (2,5-DHBA, model shown in Figure 1a) on the (10.4) cleavage plane of calcite (model shown in Figure 1b).^[30] In this system, a temperature-driven structural transition has been experimentally observed from a so-called striped to a dense phase.^[31] This transition has recently been elucidated in detail using density functional theory,^[30] unraveling the individual transition steps. The striped phase is composed of hydrogen-bonded molecular dimers and the dense phase of molecular monomers. Therefore, the formation of the dense phase has been shown to be associated with the dissociation of the dimers. While the dissociation of an isolated hydrogen-bonded dimer on the surface is associated with a high energy barrier, the corresponding process has been shown to be facilitated by the presence of a dense island, reducing the barrier to only 0.7 eV.

This is why this decisive step is referred to as attachment-assisted dimer dissociation. Obviously, it is highly desirable to benchmark this theoretical result against an experimental validation, especially because many benzoic acid derivatives are known to form dimers in the bulk phase. Experimentally, however, the barrier of this decisive dissociation step is difficult to determine as many factors—such as space limitations and capture zone depletion—are known to influence or even suppress this process. Therefore, it is important to carefully exclude the effect of such factors when aiming for a meaningful measurement of the respective rates. The generic strategy presented here can be adopted to other systems where the kinetics depends on multiple factors.

Here we demonstrate that the experiment can be performed in a way that we eliminate the influence of all known factors on the transition rate except for the temperature dependence. This approach allows for extracting the barrier for this individual step exclusively. While we present the disentanglement for the specific system of 2,5-DHBA on calcite (10.4), the proposed approach is applicable to other systems as well and, therefore, is of more general nature. The disentanglement is mandatory for a direct comparison of experimental and theoretical results and constitutes the fundament for providing molecular-level insights into the transition mechanism.

In the gas phase, 2,5-DHBA is known to form dimers^[30] like in the bulk. Therefore, upon sublimating the molecules onto the calcite (10.4) surface, dimers will be deposited. In this work, we sublimated the molecules onto calcite held at about 100 K and studied the structures that form as a function of substrate temperature. Dynamic atomic force microscopy (AFM) images taken after low-coverage deposition reveal streaky features, indicative of mobile dimers. Below 260 K these dimers form molecular islands on the surface (see Figure 2, left inset in a), which—due to their striped inner structure—are referred to as striped islands.^[31] As detailed in the Supporting Information, the striped islands are in equilibrium with the mobile dimers. When increasing the substrate temperature above ≈ 260 K, mobile dimers start to form a further type of island, the so-called dense islands (see Figure 2, right inset in a). Thereby “consumed” mobile dimers are “refilled” by dimers detaching from the striped islands, keeping the concentration of mobile dimers constant at $0.3 \text{ dimers nm}^{-2}$ (see Figure S2 in the Supporting Information). As a consequence, the area covered by striped islands shrinks, while the area covered by the dense islands grows.

Interestingly, the dense islands are built by molecular monomers rather than dimers. Therefore, the formation of the dense islands requires the dimers to dissociate, explaining why this transition is only observed for temperatures above ≈ 260 K.

The aim of the present study is to validate the theoretically obtained dissociation barrier of 0.7 eV^[30,31] by obtaining an experimental counterpart of this barrier. However, simply monitoring the increase in dense island area would result in measuring a false dimer dissociation barrier, because the increase in the dense island area depends on various factors and, therefore, is not exclusively governed by temperature. Hence, we first need to identify the factors impacting the transition rate of the step of interest. Second, we then design the experiment in a way that these factors remain unchanged throughout the measurement. Finally, temperature-dependent

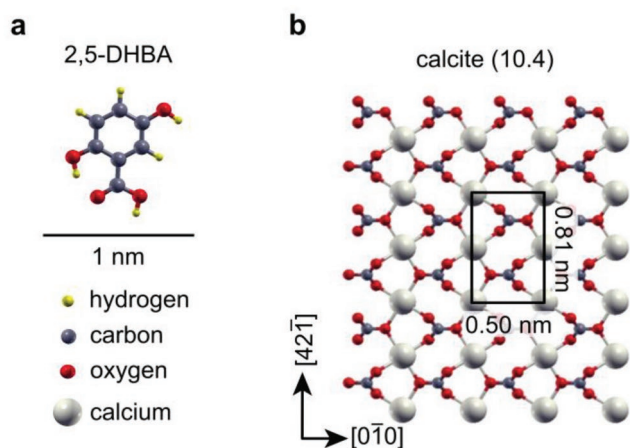


Figure 1. Model of a) the 2,5-DHBA molecule and b) the calcite (10.4) surface studied here. The scale bar applies to both panels.

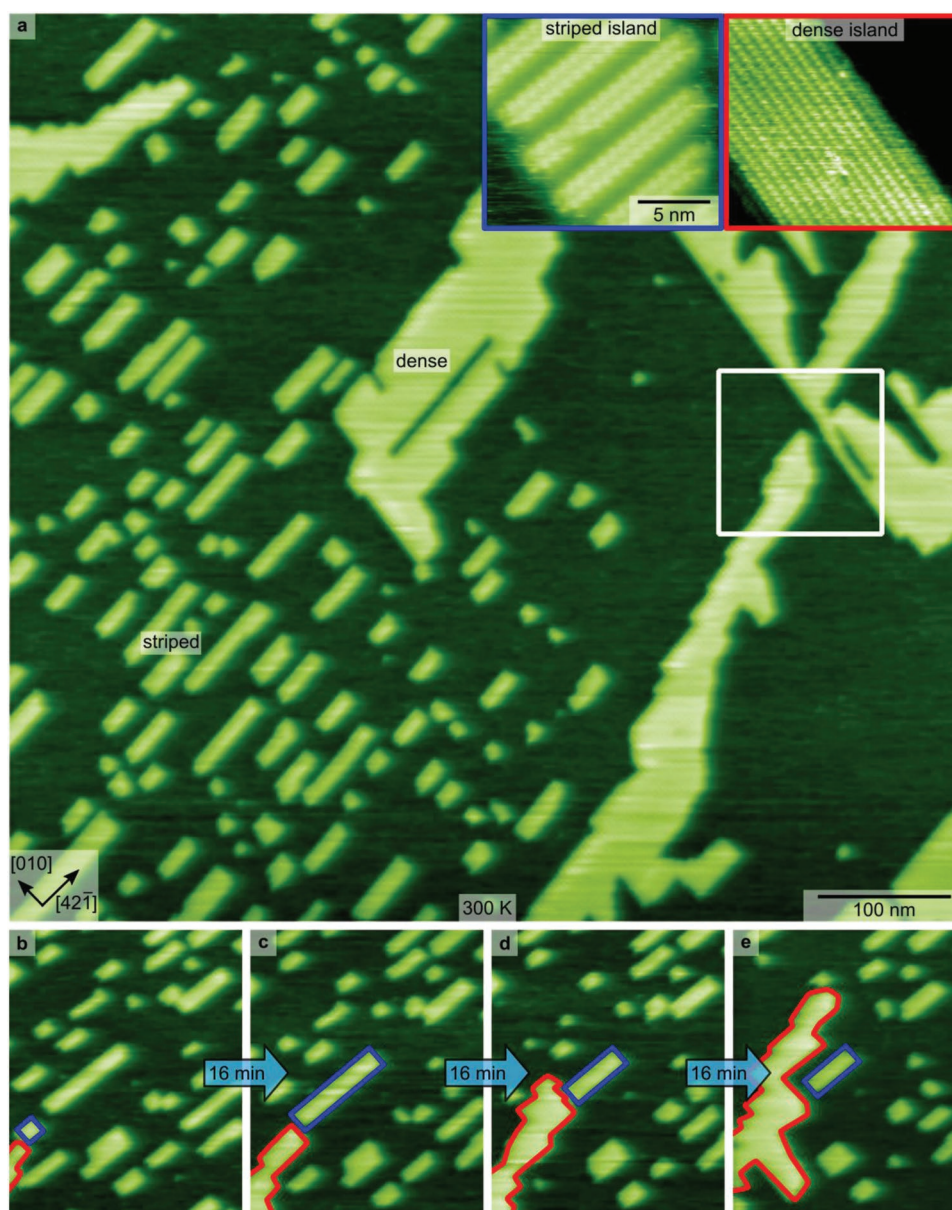


Figure 2. Dynamic AFM images that elucidate factors affecting the transition rates. In these images, both striped and dense islands are seen. Due to the large scan area, the two islands types appear rather similar. However, zooming onto the respective islands allows for unambiguous identification of striped (see left inset with blue frame in (a)) and dense (see right inset with red frame in (a)) islands. a) In an area where the growing edge of a dense island approaches an already existing dense island (marked by a white rectangle), the growth is ultimately stopped due to space limitation (#2). Also note the depletion of the area around the dense island: The formation of dense islands apparently consumed the striped islands in the proximity, resulting in a capture zone depletion (#3). b–e) Image series revealing the growth of a dense island (marked by the red perimeter). When a striped island is approached (marked by the blue perimeters), the dense island partly circumvents the striped island. In the course of the process, the stripe island is gradually consumed.

measurements are taken and the temperature-dependent transition rates are obtained.

In the following, we discuss the relevant factors and present our strategies to rule out their influence on the rate determination.

First, the dimer dissociation rate should scale with the concentration of mobile dimers (#1). As discussed above, the concentration of mobile dimers is maintained at a constant value as long as striped islands are still present on the surface. Thus,

to ensure a constant mobile dimer concentration, a necessary yet not sufficient (see below #3) condition is an excess of striped islands.

Second, the inspection of image series revealed that the dense island growth occurs predominantly at a specific island edge, whose normal vector is aligned along the $[42\bar{1}]$ surface direction. Consequently, the growth rate is affected by the accessibility of the mobile dimers to this specific edge. When other islands (striped or dense) are blocking this growing edge of the

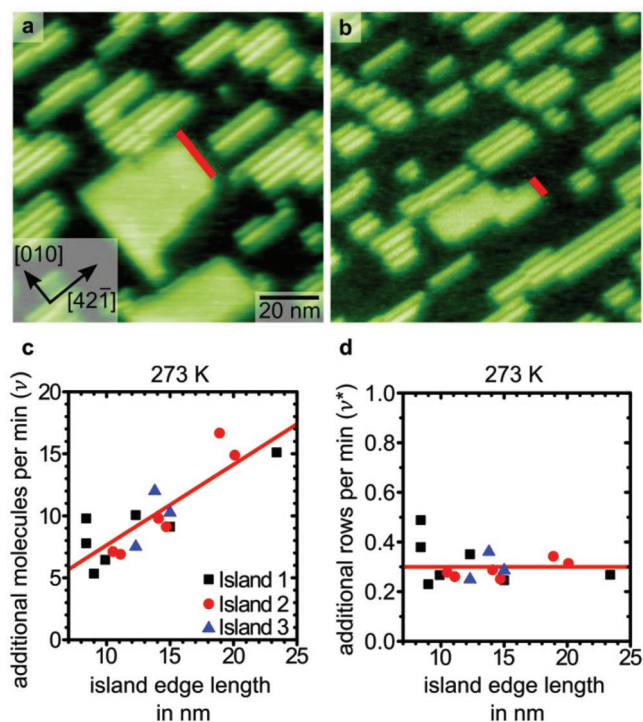


Figure 3. Dynamic AFM images to explain the dependence of the measured rates v on the island edge length (#4). From the experiments, we find that the dense islands grow predominantly from the edge (marked in red) with the normal vector oriented in the $[42\bar{1}]$ direction. In a), a longer growing edge is seen as compared to b). c) The growth of three different islands is observed at 273 K. The experimentally obtained rates (in terms of additional molecules per time step) are found to be proportional to the island edge length. Therefore, we divide the number of additional molecules by the length of the island edge (i.e., we effectively count the number of newly formed rows per time step) to obtain the transition rate v^* that is found to be independent of the island edge length d).

given island, its growth is effectively halted by a space limitation (#2, illustrated in Figure 2a). In the case of a dense island blocking, the growth is ultimately stopped (Figure 2a). In the case of a striped island blocking, the growth can be resumed as soon as the striped island has dissolved (Figure 2b–e). To avoid that space limitations affect the rate determination, we must ensure that exclusively islands with sufficient growth area are considered.

Third, the capture area in the vicinity of the growing edge might be depleted from mobile dimers (Figure 2a), when the constant equilibrium concentration of mobile dimers is not regained fast enough. This local capture area depletion (#3) can occur when equilibrium is not reached, e.g., when surrounding islands hinder mobile dimers from entering the capture area or when striped islands are far away as compared to the diffusivity. Therefore, when measuring transition rates, the islands that are monitored in time for the rate measurement were carefully chosen not to be affected by this effect.

Fourth, as the transition is known to be assisted by the presence of the dense phase, the size of the already existing dense islands must be considered. To be precise, the molecule attachment rate should scale with the growing edge length (#4). As shown in Figure 3a,b, the islands vary in their edge length. In

addition, time-dependent measurements indicate that the edge length of a single island can also change in time. The experimental observations indeed confirm that the molecule attachment rate is proportional to the growing edge length of the dense island (see Figure 3c). To take this effect into account and be able to compare the rate with the individual one that was calculated theoretically,^[30] we divide the counted number of newly attached molecules by the growing edge length. This procedure eventually results in a transition rate $v^*(T)$ that unravels the kinetics solely of the desired dimer dissociation step (Figure 3d); see the Supporting Information for the rigorous justification of this procedure.

Finally, we need to confirm that the above four factors cover all aspects that influence the transition rate. To this end, we validate that the measured growth rates are constant at constant temperature (see Figure S3 in the Supporting Information).

After having clarified the factors that impact the transition rate measurements, we performed temperature-dependent dynamic AFM image series following the growth of carefully chosen, individual dense islands. A typical representation is shown in Figure 4, which illustrates the data collection at a substrate temperature of 276 K. Two consecutive images with a time delay of 16 min (Figure 4a,b) are compared by generating a difference image (Figure 4c), that highlights vanishing (blue) and appearing (red) structures.

In the images, an abundance of striped, as compared to dense, islands can be seen, which are expected to effectively refill the concentration of mobile dimers (addressing #1). Thus, the concentration of mobile dimers is assumed to remain constant, which, in turn, means that the obtained rate is independent of the total molecular coverage. The striped islands are observed to both shrink and grow at both ends, indicating that the detachment from the striped islands is not the rate-limiting step. Mobile dimers are visible by the streaks that cover the otherwise bare surface areas. Near the center of the image, a single dense island exists, which is the island under investigation. We confirm that the growing edge in the upper right part of the island is not blocked by other islands (#2) and that the capture zone surrounding the growing edge is not fenced in by other islands (#3). From the difference image in Figure 4c we can clearly identify the growing edge of the dense island, which is the edge in the upper right part of the island. As outlined above, we finally divide the number of newly attached monomers by the length of the growing edge (#4) to arrive at a valid representation of the transition rate that is constant at the given temperature. Due to the careful design of the experiment, the determination of the rate is now reduced to the essential step, namely the attachment-assisted dimer dissociation barrier.

Following the route described here, we determined the transition rates at various temperatures. Each rate measurement was performed using image series composed of several images. For high rates (i.e., high temperatures), a measurement time of about 1 h was sufficient, while small rates (i.e., low temperatures) required measurement times of more than 4 h. As we have limited the process to the temperature dependence solely, we can now make use of a simple Arrhenius plot for extracting the energy barrier (see the Supporting Information for details on the procedure). The resulting plot is given in Figure 5.

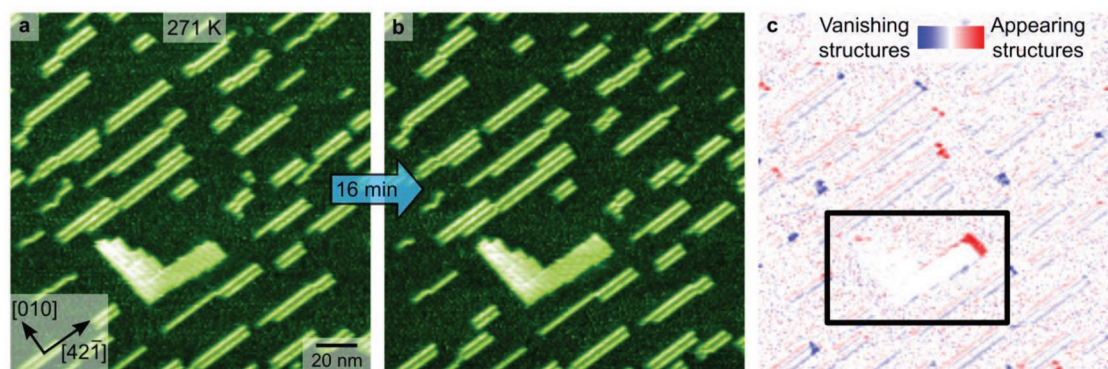


Figure 4. Illustration of the growth rate determination. a) Dynamic AFM image taken at a substrate temperature of 271 K. The surface is covered with striped islands, a single angle-shaped dense island near the center and mobile dimers. b) Image acquired 16 min after the image shown in (a) using the same imaging conditions. c) Difference image illustrating the growth of the dense island at the upper island edge, the growth in other directions is substantially smaller, indicating further constraints that are not considered here (the growing dense island is marked with rectangle). Striped islands are seen to shrink or grow at the ends of the stripes. Note that the images are corrected for linear drift to allow for taking a meaningful difference image. A minor nonlinear drift effect is still visible in the image, which is manifested in the faint blue regions to the lower right and the red regions to the upper left of all features. These faint regions are, therefore, artefacts from nonlinear drift.

From the Arrhenius plot in Figure 5, we are now able to extract the pre-exponential factor and the energy barrier for the single step of interest, namely the attachment-assisted dimer dissociation. The calculated pre-exponential factor is $1.9 \pm 0.1 \times 10^{12}$ 1/s, while the energy barrier was found to be (0.8 ± 0.1) eV. This experimental value compares excellently with the calculated value of 0.7 eV for the attachment-assisted dimer dissociation as obtained from density-functional theory. This direct comparison is possible only because of the disentanglement approach presented here, allowing for extracting the barrier of an individual transition step within a rather complex sequence of steps. The excellent agreement between experiment and theory corroborates the picture drawn based on the calculations and the experimental observations. Our results contribute to an in-depth understanding of the process at the molecular level.

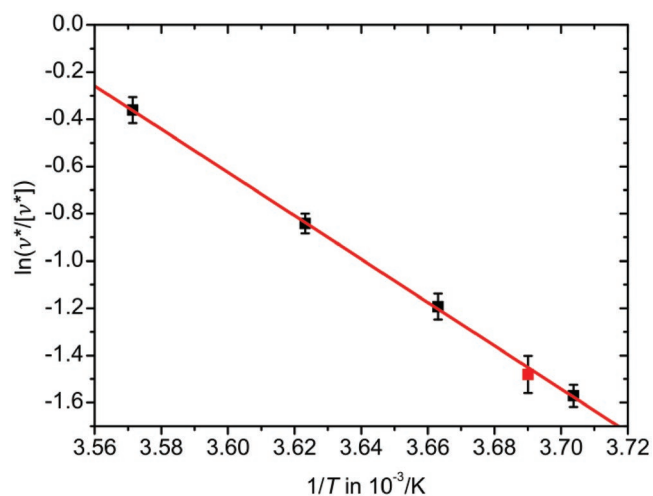


Figure 5. Arrhenius plot of the transition rate constant as a function of inverse substrate temperature. Except for the data point marked in red, all data points shown here are collected on the same sample. We reproduced the results with a new sample (271 K). The stated errors are the calculated standard errors of the mean.

The structural transition of 2,5-DHBA on calcite (10.4) from a so-called striped to a dense phase is composed of a sequence of individual transition steps. To obtain molecular-level insights into the underlying atomistic mechanism, we demonstrate our new disentanglement approach by precisely analyzing the transition process based on dynamic AFM image series. These experimental data disclose factors that impact the transition kinetics from mobile dimers to the dense phase, including space limitations, capture zone depletion and the length of the growing edge. By carefully excluding these factors, their impact on the measured rates is eliminated, hence exclusively the dependence of the transition rate on temperature is left. These experimental insights allow for exclusively extracting the temperature-dependent rates for a single step, namely the decisive attachment-assisted dimer dissociation. Our results reveal a transition barrier of 0.8 eV, which agrees well with the theoretical result of 0.7 eV. This study demonstrates how a complex process can be analyzed by limiting the investigation to a single, essential transition step and extracting detailed information exclusively for this individual transition.

Experimental Section

All dynamic AFM measurements shown in this work were carried out with a Scienta Omicron VT AFM XA operated in the frequency modulation mode as described elsewhere.^[31] N-doped silicon cantilevers were used from Nanosensors with a nominal force constant of 40 N m^{-1} and an eigenfrequency of 300 kHz in UHV. The images shown here were taken with a scan speed of 2 lines per second, which means that one image (trace and retrace) with 500×500 pixel takes about 8 min. Sample preparation as well as molecule deposition were performed in situ with a chamber base pressure typically better than 10^{-10} mbar. Optical quality calcite (CaCO_3) crystals were purchased from Korth Kristalle GmbH, Kiel, Germany. The 2,5-DHBA molecules were bought from Aldrich, Munich, Germany. Molecule deposition was done using a home-built Knudsen cell that is heated to $\approx 70^\circ \text{C}$ for molecule sublimation. For the experiments shown here, a sublimation time of 10 min onto a sample at a distance of ≈ 9 cm was used. To ensure that the scanning process does not affect the observed kinetics, experiments were performed comparing

the situation after continuous scanning and after having paused the scanning process. Moreover, imaging at different setpoints, i.e., different tip-sample distances did not result in different kinetics, which further indicates that the scanning does not influence the transition process.

Supporting Information

Supporting Information is available from the Wiley Online Library or from the author.

Acknowledgements

The manuscript was written through contributions of all authors. All authors have given approval to the final version of the manuscript. Most stimulating discussions with Maximilian Vogtland and Martin Aeschlimann are gratefully acknowledged. S.A. is a recipient of a DFG-fellowship through the Excellence Initiative by the Graduate School Materials Science in Mainz (GSC 266).

Conflict of Interest

The authors declare no conflict of interest.

Keywords

Arrhenius, atomic force microscopy, energy barrier, nanoscience, surface science

Received: May 6, 2019
Revised: July 12, 2019
Published online:

- [1] D. I. Rogilo, L. I. Fedina, S. S. Kosolobov, B. S. Rangelov, A. V. Latyshev, *Phys. Rev. Lett.* **2013**, *111*, 036105.
- [2] R. D. Smith, R. A. Bennett, M. Bowker, *Phys. Rev. B* **2002**, *66*, 7.
- [3] Y. Han, S. M. Russell, A. R. Layson, H. Walen, C. D. Yuen, P. A. Thiel, J. W. Evans, *Phys. Rev. B* **2013**, *87*, 155420.
- [4] S. Schauermann, H. J. Freund, *Acc. Chem. Res.* **2015**, *48*, 2775.
- [5] H. Schwarz, *Catal. Sci. Technol.* **2017**, *7*, 4302.
- [6] P. Z. Chen, T. P. Zhou, S. B. Wang, N. Zhang, Y. Tong, H. X. Ju, W. S. Chu, C. Z. Wu, Y. Xie, *Angew. Chem., Int. Ed.* **2018**, *57*, 15471.
- [7] A. Saywell, J. Schwarz, S. Hecht, L. Grill, *Angew. Chem., Int. Ed.* **2012**, *51*, 5096.
- [8] A. Johnson-Buck, J. Nangreave, S. Jiang, H. Yan, N. G. Walter, *Nano Lett.* **2013**, *13*, 2754.
- [9] P. Tegeder, *J. Phys.: Condens. Matter* **2012**, *24*, 394001.
- [10] C. Nacci, M. Baroncini, A. Credi, L. Grill, *Angew. Chem., Int. Ed.* **2018**, *57*, 15034.
- [11] D. Spitzer, V. Marichez, G. J. M. Formon, P. Besenius, T. M. Hermans, *Angew. Chem., Int. Ed.* **2018**, *57*, 11349.
- [12] S. Ditze, M. Stark, M. Drost, F. Buchner, H. P. Steinrück, H. Marbach, *Angew. Chem., Int. Ed.* **2012**, *51*, 10898.
- [13] M. Lepper, J. Köbl, L. Zhang, M. Meusel, H. Hölzel, D. Lungerich, N. Jux, A. de Siervo, B. Meyer, H. P. Steinrück, H. Marbach, *Angew. Chem., Int. Ed.* **2018**, *57*, 10074.
- [14] G. Ertl, *Angew. Chem., Int. Ed.* **2008**, *47*, 3524.
- [15] T. R. Linderroth, S. Horch, E. Lægsgaard, I. Stensgaard, F. Besenbacher, *Phys. Rev. Lett.* **1997**, *78*, 4978.
- [16] M. Schunack, T. R. Linderroth, F. Rosei, E. Lægsgaard, I. Stensgaard, F. Besenbacher, *Phys. Rev. Lett.* **2002**, *88*, 156102.
- [17] J. Weckesser, J. V. Barth, K. Kern, *J. Chem. Phys.* **1999**, *110*, 5351.
- [18] J. V. Barth, *Surf. Sci. Rep.* **2000**, *40*, 75.
- [19] K. Balashev, N. J. DiNardo, T. H. Callisen, A. Svendsen, T. Bjornholm, *Biochim. Biophys. Acta, Biomembr.* **2007**, *1768*, 90.
- [20] H. L. Wu, L. Yu, Y. J. Tong, A. M. Ge, S. Yau, M. Osawa, S. Ye, *Biochim. Biophys. Acta, Biomembr.* **2013**, *1828*, 642.
- [21] S. Jaekel, A. Richter, R. Lindner, R. Bechstein, C. Nacci, S. Hecht, A. Kühnle, L. Grill, *ACS Nano* **2018**, *12*, 1821.
- [22] K. Celebi, M. T. Cole, J. W. Choi, F. Wycisk, P. Legagneux, N. Rupesinghe, J. Robertson, K. B. K. Teo, H. G. Park, *Nano Lett.* **2013**, *13*, 967.
- [23] C. F. He, S. W. Shi, X. F. Wu, T. P. Russell, D. Wang, *J. Am. Chem. Soc.* **2018**, *140*, 6793.
- [24] E. Reimhult, F. Höök, B. Kasemo, *Phys. Rev. E* **2002**, *66*, 051905.
- [25] S. R. Tabaei, J. A. Jackman, S.-O. Kim, V. P. Zhdanov, N.-J. Cho, *Langmuir* **2015**, *31*, 3125.
- [26] B. T. Richards, S. R. Schraer, E. J. McShane, J. Quintana, B. D. A. Levin, D. A. Muller, T. Hanrath, *Chem. Mater.* **2017**, *29*, 4792.
- [27] S. S. Chae, S. Jang, W. Lee, D. W. Jung, K. H. Lee, J. D. Kim, D. Jeong, H. Chang, J. Y. Hwang, J.-O. Lee, *Small* **2018**, *14*, 1801529.
- [28] J. Seo, J. Lee, G. Jeong, H. Park, *Small* **2019**, *15*, 1804133.
- [29] H. M. Zhang, J. H. Franke, D. Y. Zhong, Y. Li, A. Timmer, O. D. Arado, H. Monig, H. Wang, L. F. Chi, Z. H. Wang, K. Mullen, H. Fuchs, *Small* **2014**, *10*, 1361.
- [30] C. Paris, A. Floris, S. Aeschlimann, J. Neff, F. Kling, A. Kühnle, L. Kantorovich, *Commun. Chem.* **2018**, *1*, 66.
- [31] C. Paris, A. Floris, S. Aeschlimann, M. Kittelmann, F. Kling, R. Bechstein, L. Kantorovich, A. Kühnle, *J. Phys. Chem. C* **2016**, *120*, 17546.